Structural Engineering and Mechanics, *Vol. 64, No. 6 (2017) 803-817*
DOI: https://doi.org/10.12989/sem.2017.64.6.803

Damage detection for a beam under transient excitation via three different algorithms

Ying Zhao[1], Mohammad Noori*[1,2] and Wael A. Altabey[1,3]

[1]*International Institute for Urban Systems Engineering, Southeast University, Nanjing, 210096, China*
[2]*Mechanical Engineering, California Polytechnic State University, San Luis Obispo, California 93405, USA*
[3]*Department of Mechanical Engineering, Faculty of Engineering, Alexandria University, Alexandria 21544, Egypt*

(Received December 27, 2016, Revised September 28, 2017, Accepted October 11, 2017)

Abstract. Structural health monitoring has increasingly been a focus within the civil engineering research community over the last few decades. With increasing application of sensor networks in large structures and infrastructure systems, effective use and development of robust algorithms to analyze large volumes of data and to extract the desired features has become a challenging problem. In this paper, we grasp some precautions and key points of the signal processing approach, wavelet, establish a relative reliable framework, and analyze three problems that require attention when applying wavelet based damage detection approach. The cases studies how to use optimal scales for extracting mode shapes and modal curvatures in a reinforced concrete beam and how to effectively identify damages using maximum curves of wavelet coefficient differences. Moreover, how to make a recognition based on the wavelet multi-resolution analysis, wavelet packet energy, and fuzzy sets is a meaningful topic that has been addressed in this work. The relative systematic work that compasses algorithms, structures and evaluation paves a way to a framework regarding effective structural health monitoring, orientation, decision and action.

Keywords: mode shape; curvature mode; wavelet coefficient differences; multi-resolution analysis; damage identification; artificial neural network; fuzzy pattern recognition; reinforced concrete beam

1. Introduction

Increased awareness of the economic and societal effects of aging, deterioration and extreme events on civil infrastructure systems have become a major concern and the focus of a significant volume of research studies. How to most effectively address the integrity, safety, resilience, and reliability of infrastructure and to circumvent potential catastrophic failure is important to the wellbeing of any society. Importantly, advanced signal processing methods applied to study and diagnose the damage detection and deterioration of structural elements under dynamic loads are becoming key methodologies in the structural analysis and health monitoring of major structural systems (Chang *et al*. 2003). Classical signal processing has been mainly focused on the design of time-invariant and space-invariant operators and modifying the basic stationary signal properties. Concentrating on transients has become the strategy for grasping significant information from the overwhelming amount of data recorded by sensors (Mallat 1999).

Wavelet transform is a tool that separates data or functions or operators into different frequency components, and studies each component with a specific resolution matched to its scale (Daubechies 1992). Compared with other signal processing methods that encompass short-time, windowed Fourier transform, wavelet transform has demonstrated to be more effective for its precise measurement using time-frequency localization technique (Daubechies 1990). Wavelet analysis has also attracted attention for its ability to analyze rapidly changing transient signals (Lee and Yamamoto 1994). Its features prove a great success in a widespread range of practical applications including the speech processing realm such where the signal can be efficiently reconstructed after coding or identified for recognition (Farouk 2014). Due to versatile characteristics and properties of wavelets, in this paper a wavelet based strategy is utilized for damage identification in a reinforced concrete beam utilizing its mode shapes and modal curvatures. Subsequently, we demonstrate how to make fuzzy recognition for the beam under external transient load.

2. Mode shape based damage identification

A large volume of research has been reported on the utilization of wavelet transform for damage detection over the past two decades. Some of those studies that have been the motivation for the work presented herein are summarized in this section.

A pilot study was conducted using a severely damaged square plate under harmonic response (Beheshti-Aval *et al*. 2013). Several criteria and cases such as the smallest size damage that can be detected, correlation between the crack width and the number of sampling points, and the influence of the damage thickness on the accuracy of the result were

*Corresponding author, Professor
E-mail: yzhseu@gmail.com

ISSN: 1225-4568 (Print), 1598-6217 (Online)

investigated. The vibration mode of a cracked plate was transformed with wavelet, and both the location and extent of the crack were accurately described and quantitatively estimated (Loutridis *et al*. 2005). A Plexiglas cantilever beam and a steel plate with four fixed boundary conditions were tested experimentally, and the damage locations were estimated using mode shapes as a damage index in a wavelet-based analysis (Rucka and Wilde 2006). The fundamental vibration mode of a cracked cantilever beam was analyzed using continuous wavelet transform and both the location and size of the crack were estimated (Douka *et al*. 2003). According to the fundamental vibration mode of a double-cracked cantilever beam, the location of the cracks was detected by sudden changes in the spatial variation of the wavelet transformed response. The relative depth was estimated when relating the intensity factor to the wavelet coefficients (Loutridis *et al*. 2004).

Different types of wavelets were used to analyze the first vibration mode of a plate with two all-over part-through cracks. The sensitivity of the wavelet transform method with respect to the type, scale of wavelets, the variation in distance between two cracks and relative depth of cracks were investigated (Nikravesh *et al*. 2013). The efficiency of the applied wavelets was verified by analytically and experimentally determined data using static deflection of a beam according to the spatially distributed points obtained by processing digital photographs, and thus the cracks were localized (Rcka and Wilde 2006).

The magnitude of the Lipschitz exponent could be used as an indicator of damage extent for a fundamental vibration of a beam by choosing suitable wavelet (Hong *et al*. 2002). The local perturbations caused by damage can be discernible from component wavelets, and this was demonstrated by numerically simulated deflection responses of a uniform beam containing a short transverse crack under both static and dynamic loading conditions. Moreover, in the same study smooth analytical crack-tip displacement fields were also used for further verification (Wang and Deng 1999).

A distributed two-dimensional (2D) Continuous Wavelet Transform (CWT) algorithm was developed which can use data from discrete sets of nodes and provide spatially continuous variation in the structural response parameters to monitor structural degradation. The feasibility of the method was demonstrated based on the crack-tip strain field of a plate subjected to bi-axial loads, and the deflection field of a simply supported plate with defects subjected to static or impacting transverse loads (Huang *et al*. 2009).

Stationary wavelet transform multi-resolution analysis (SWT-MRA) was used to refine the uniform load surface (ULS) obtained from the damaged structure and then using continuous wavelet transform for localizing the discontinuity of improved ULS as a sign of damage location (Masoumi and Ashory 2014). Different crack characteristics such as length, width, orientation, depth, structural boundary conditions, and corresponding wavelet types were investigated for beam structures (Quek *et al*. 2001). Curvatures and continuous wavelet transforms (CWTs) of differences between a measured mode shape of a damaged beam and that from a polynomial that fitted the MS of the damaged beam were processed to yield a curvature damage index (CDI) and a CWT damage index, were respectively evaluated (Xu *et al*. 2014). It was also proven that the local maxima of wavelet transform modulus can detect the locations of irregular structures and provide numerical procedures to compute the corresponding *Lipschitz* exponents (Mallat and Hwang 1992).

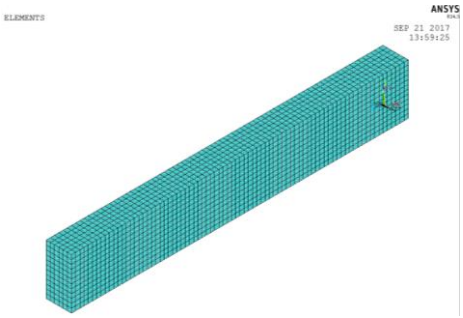

Fig. 1 Reinforced concrete beam analytical model

The simulation response data were generated from the ASCE structural health monitoring benchmark subjected to stochastic wind loading. A wavelet-based approach was developed that could accurately identify the damage introduced by breaking one or more structural elements such as the interstory braces, and determined by the spatial distribution pattern of the observed spikes (Hera and Hou 2004). A wavelet based approach was also applied to simulation data generated from structural model consisting of multiple breakable springs, where some suffered irreversible damage and exceeded their fatigue life subjected to a harmonic excitation.

Therefore, as demonstrated in the summary of several research studies utilizing wavelet for damage detection, wavelet has shown great promise in damage identification and structural health monitoring (Hou and Noori 2000).

2.1 Numerical simulation procedure

In this study, a reinforced concrete beam modeled by finite element is considered. The beam is simply supported on both sides. The basic geometric dimensions of the beam are L=2 m, B=0.15 m, H=0.3 m, and the analytical model can be seen in Fig. 1. Different damage conditions are simulated according to the corresponding situation. For instance, m/8L indicates crack happens at the m^{th} location, while n/8H indicates the specific nth crack depth relative to the beam height H at length (Tables 1-3). Damage is simulated using stiffness reduction.

Table 1 Reinforced concrete beam structure

Material	Type	Elasticity Modulus	Poisson Ratio	Density
Concrete	C30	30GPa	0.2	2550 kg/m^3
Rebar	HRB400	200GPa	0.3	7800 kg/m^3

Table 2 Damage location (range)

0/8L	1/8L	2/8L	3/8L	4/8L
0 m	0.25 m	0.5 m	0.75 m	1 m
-0.025 m	-0.275 m	-0.525 m	-0.775 m	-1.025 m

Table 3 Damage depths at the same location

1/12H	2/12H	3/12H	4/12H
0.025 m	0.05 m	0.075 m	0.10 m

2.2 Force analysis

For a typical beam structure, a crack or a defect in a section can be regarded as an abrupt stiffness change in the structure. In this section, we derive the bound of *Lipschitz* exponent using the simplest Euler beam theory.

The rigorous analysis of the *Lipschitz* exponent may have to be carried out by the exact elasticity theory, and we employ dense points to naturally simulate the real state of damaged beam, satisfying Euler beam theory. When applying Euler beam theory, the field variables are displacement, rotation, moment and shear force. If one denotes by $x=v$ the point of an abrupt thickness change in a beam, one can state clearly the continuity condition across the discontinuity as

$$\text{Displacement: } w(v^+) = w(v^-) \tag{1}$$

$$\text{Rotation: } \frac{dw(v^+)}{dx} = \frac{dw(v^-)}{dx} \tag{2}$$

$$\text{Moment: } EI(v^+)\frac{d^2w(v^+)}{dx^2} = EI(v^-)\frac{d^2w(v^-)}{dx^2} \tag{3}$$

$$\text{Shear Force: } EI(v^+)\frac{d^3w(v^+)}{dx^3} = EI(v^-)\frac{d^3w(v^-)}{dx^3} \tag{4}$$

Where the subscripts + and - are used to denote if the specific quantity is at the right or the left side of the discontinuous point. The magnitude of the *Lipschitz* exponent, derived from wavelet transform, is used as a useful and effective indicator of the damage extent when appropriate wavelet basis is chosen.

2.3 Wavelet transform

Continuous wavelet transform (CWT) is the process of signal shifting and scaling continuously with acquired sampled data. Shifting process is a smoothing effect through the full length of the sampled data, while scaling process can be chosen from the minimum scale to the maximum scale, indicating various resolutions. The trade-off of improved resolution is between increased computational time and memory by calculating wavelet coefficients, and multiplying each coefficient by the appropriately scaled and shifted wavelet, which yields the constituent wavelet of the original signal.

Continuous wavelet transform is defined by

$$W_f(a,b) = \langle f, \psi_{ab}\rangle = |a|^{-1/2}\int_{-\infty}^{+\infty} f(x)\overline{\psi\left(\frac{x-b}{a}\right)}dx \tag{5}$$

Where: $(W_f)(a,b)$ is the wavelet coefficient, and a and b are continuously varying. Wavelet coefficient represents how closely correlated the wavelet is with the section of the signal. The higher the coefficient is, the more the similarity is. The equivalent frequency domain representation is

$$W_f(a,b) = \frac{\sqrt{a}}{2\pi}\int_{-\infty}^{+\infty}\hat{x}(\omega)\overline{\hat{\psi}(a\omega)}e^{iwb}d\omega \tag{6}$$

Inverse continuous wavelet transform (ICWT) holds if and only if satisfying the admissibility condition.

$$f(x) = \frac{1}{C_\psi}\int_{-\infty}^{+\infty}\int_{-\infty}^{+\infty}\frac{1}{a^2}W_f(a,b)\,\psi_{ab}(x)dadb \tag{7}$$

2.4 Time-frequency characteristics

Wavelet transform provides a time-frequency picture, with, potentially, good localization properties in both "time" and "frequency" variables. Wavelet function $\psi(x)$ is generally oscillated in the time domain under the admissibility condition, and its Fourier transform $\hat{\psi}(\omega)$ is a band-pass function, both with good capability in detecting local properties. If x^* and Δ_x denote respectively the center location and radius of $\psi(x)$, and ω^* and Δ_ω denote respectively the center frequency and radius of $\hat{\psi}(\omega)$, the center location and radius of $\psi_{ab}(x)$ are ax^*+b and a Δ_x respectively, and the center and radius of $\hat{\psi}_{ab}(\omega)$ are ω^*/a and Δ_ω/a respectively. The value of Δ_x and Δ_ω are mutually constrained, satisfying *Heisenberg Uncertainty Principle*. The time-frequency characteristic spectrum of wavelet analysis is shown in Figs. 2 and 4 and Figs. 3 and 5 by two groups of generated signals, each integrating four different frequencies and corresponding phases with 10% Gaussian noise. (Note: PSD-TISA indicates Power Spectral Density-Time Interval Squared Amplitude).

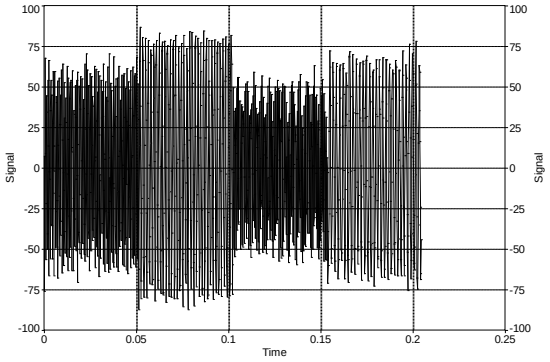

Fig. 2 Generated signal (1)

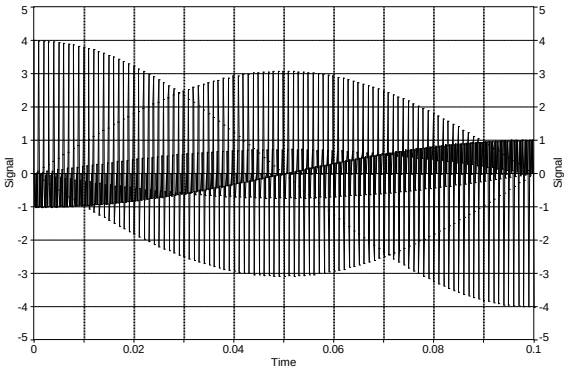

Fig. 3 Generated signal (2)

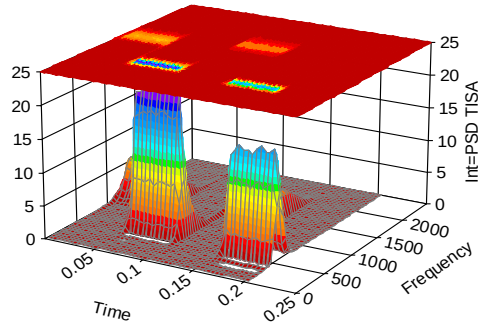

Fig. 4 WT time-frequency spectrum (1)

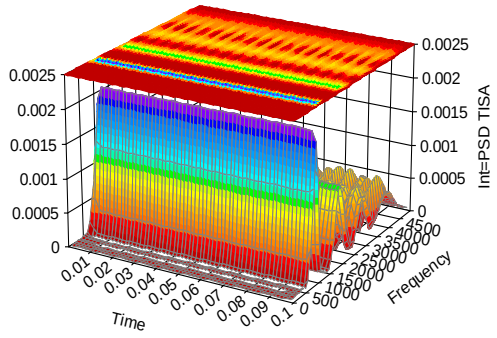

Fig. 5 WT time-frequency spectrum (2)

As briefly mentioned above, when the scale a increases, the length of $\psi_{ab}(x)$ increases, and the resolution of time domain decreases in the time domain, while the center and the length of $\hat{\psi}_{ab}(\omega)$ decreases, and the resolution of frequency domain accordingly increases in the frequency domain. In this case, when the scale is large, the low frequency components of the signal are analyzed using high frequency domain resolution and low time frequency resolution. When the scale a decreases, the length of $\psi_{ab}(x)$ decreases, and the resolution of time domain increases in the time domain, while the center and the length of $\hat{\psi}_{ab}(\omega)$ increases, and the resolution of frequency domain accordingly decreases in the frequency domain. In this case, when the scale is large, high frequency components of the signal are analyzed using low frequency domain resolution and high time frequency resolution.

2.5 Multi-resolution analysis

Let the square integrable function $f(x) \in L^2(\mathbb{R})$ be the limiting case of progressive approximation. Each approximation results from $f(x)$ smoothed by low-pass smoothing function $\phi(x)$, and the smoothing function $\phi(x)$ is concurrently zooming when approximating. Therefore, multi resolution analysis in $L^2(\mathbb{R})$ space is the process of a progressive decomposition of $L^2(\mathbb{R})$ space, generating a group of progressively inclusive subspaces.

$$\cdots, \mathrm{V}_0 = \mathrm{V}_1 \oplus \mathrm{W}_1, \mathrm{V}_1 = \mathrm{V}_2 \oplus \mathrm{W}_2, \cdots, \mathrm{V}_\mathrm{j} = \mathrm{V}_{\mathrm{j}+1} \oplus \mathrm{W}_{\mathrm{j}+1}, \cdots \quad (8)$$

$\forall$ scale j_0, a discrete signal $f(n)$ can be expressed as the sum of a group of orthogonal bases comprised of scaling functions at scale j_0, and all of the wavelets at scale j ($j > j_0$)

$$f(n) = \sum_k c_{j0,k}\phi_{j0,k}(n) + \sum_{j>j_0}\sum_k d_{j,k}\psi_{j,k}(n) \quad (9)$$

Where: $c_{j0,k} = \langle f(n), \phi_{j0,k}(n)\rangle$, $d_{j,k} = \langle f(n), \psi_{j,k}(n)\rangle$, and ϕ and ψ are the scaling function and wavelet function respectively. Scaling function is the equivalent of the low pass filter, and assures a smooth shape, while wavelet function is the equivalent of high pass filter, and retains the details of signal changes.

2.6 Singularity detection

The singularity detection principle has been used for a quantification approach for damage identification (Douka *et al.* 2003, Loutridis *et al.* 2005, Hong *et al.* 2002, Mallat 1999) *Lipschitz.* Index can be defined as a damage index regarding the detection of discontinuities of the signal. For $f(x)$, suppose there is a positive integer $n, n \le \alpha \le n+1$. If $\exists\, \mathrm{A} > 0$ and a polynomial $p_n(x)$ of degree n, satisfying $|f(x) - p_n(x - x_0)| \le p_n(x - x_0)^\alpha$, thus, $f(x)$ is *Lipschitz* α at x_0. In general, the larger *Lip* α is, the smoother the function is and the less singular the function will be, which means the degree of damage is small.

Supposing the *Lipschitz* index of a bounded function $f(x)$ is α at x_0, and the wavelet we choose has n+1 order vanishing moments, i.e.

$$\int_{-\infty}^{+\infty} x^k \psi(x)dx = 0, \quad 0 \le k \le n+1 \quad (10)$$

Where: $f(x)$ is applied to CWT, and the WT satisfies the following in the neighborhood of x_0

$$\begin{aligned} W_f(a,b) &= \int_{-\infty}^{+\infty} a^{-\frac{1}{2}}\psi^*\left(\frac{x-b}{a}\right)f(x)dx \\ &= \int_{-\infty}^{+\infty} a^{-\frac{1}{2}}\psi^*\left(\frac{x-b}{a}\right)[f(t) - (f(b) + c_1(x-b) + \\ &\quad c_2(x-b)^2 + \cdots + c_n(x-b)^n]dx \end{aligned} \quad (11)$$

$$\begin{aligned} W_f(a,b) &\le \int_{-\infty}^{+\infty} a^{-1/2}\left|\psi^*\left(\frac{x-b}{a}\right)\right| A|x-b|^\alpha dx \\ &= Aa^{\alpha+1/2}\int_{-\infty}^{+\infty}|\psi^*(u)||u|^\alpha du = Ka^{\alpha+1/2} \end{aligned} \quad (12)$$

Where: $\frac{t-b}{a} = u$.

It follows that, the *Lipschitz* index of the square integrable function $f(x)$ is α at x_0, $\alpha \le n$, thus, within a very small neighborhood,

$$W_f(a,b) \le Ka^{\alpha+1/2} \quad (13)$$

$$\log_2|W_f(a,b)| \le \log_2|K| + (\alpha + 1/2)\log_2 a \quad (14)$$

Where: K is a coefficient associated with wavelets, and a is the scale of WT. The singularity of $f(x)$ at x_0 is the maximum tangent slope of the curve in the logarithmic coordinate system, which can be used as an index related to *Lipschitz* index α. If $\alpha > -1/2$, the modulus maximum of WT increases as the scale increases, and if $\alpha < -1/2$, the

modulus maximum of WT decreases as the scale increases.

For a specific *Lipschitz* index α and scale a, satisfying,

$$\text{Undamaged structure: } W_{f0} = K_0 a^{\alpha+1/2} \tag{15}$$

$$\text{Damaged structure: } W_{f1} = K_1 a^{\alpha+1/2} \tag{16}$$

The difference between the two formulae can be expressed as

In the rectangular coordinate system:

$$\Delta W_f = \Delta K a^{\alpha+1/2} \tag{17}$$

ΔW_f is associated with scale a and *Lipschitz* index α: $\Delta W_f = \Delta W_f(a, \alpha)$ (18)

In the logarithmic coordinate system:

$$\log_2 |\Delta W_f| = \log_2 |\Delta K| + (\alpha + 1/2) \log_2 a \tag{19}$$

Where: $\Delta W_f = W_{f1} - W_{f0}$, indicates the wavelet coefficient differences (WCD) between the undamaged structure and damaged structure, and $\Delta K = K_1 - K_0$, indicates the WT coefficient differences between the undamaged structure and damaged structure. As can be seen from the Eqs. (13)-(19) above, for a specific scale a, ΔW_f shows an exponential function associated with α, while in the logarithmic curve, the tangential slope of the function varies with α. In this wavelet application note that analysis results in the logarithmic curve may not be satisfactory, and for details please see a recent paper by the authors (Zhao and Noori).

We can infer from the exponential curve that, the wavelet coefficient difference ΔW_f approaches zero as the scale a increases to $+\infty$. Simultaneously, the wavelet coefficient difference ΔW_f is zero as the scale a vanishes to zero. Therefore, the maximum of the curve exists between the two ends of the curve, scale $a = 0$ and scale $a = \infty$, where the WT coefficient difference converges to zero. This means that the maximum modulus difference of the wavelet coefficients increases as the scale increases, and it reaches a maximum value as the scale reaches a specific value, and the difference gradually decreases as the scale continues to increase. Getting rid of the discontinuity effect, the importance of this property should be considered.

2.7 Mode shape based damage identification

Using the difference between wavelet coefficients at scale 1 to 16 (db2, fundamental mode shapes of undamaged and damaged structures), the damages in the reinforced concrete beam are identified in Fig. 6, depicting four different extents (1/12H to 4/12H damage depth) of damage at 3/8L of the beam.

According to the singularity detection principle as derived above, the damage quantification related index (wavelet coefficient differences) can be expressed as the function of *Lipschitz* index α and scale a. The maximum points of mode shape wavelet transform (db2) coefficient differences at scale 1 to 1024 can be linked to a maximum curve (MC) in Fig. 7 in the general coordinate system.

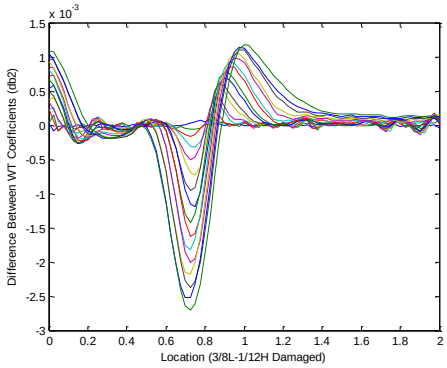

(a) 1/12H damaged

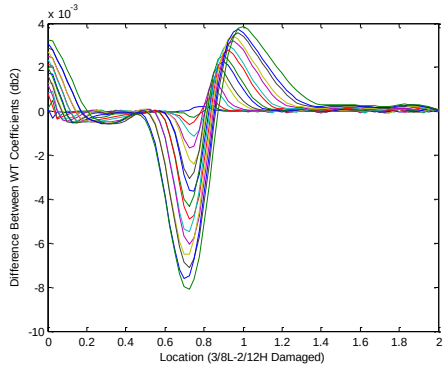

(b) 2/12H damaged

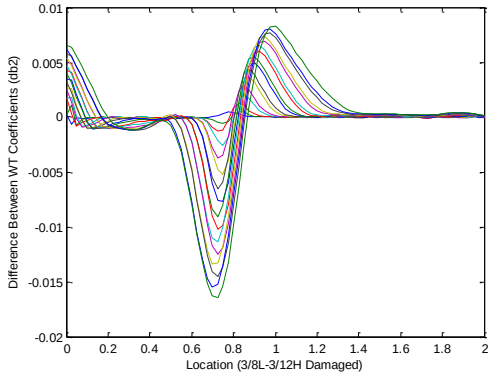

(c) 3/12H damaged

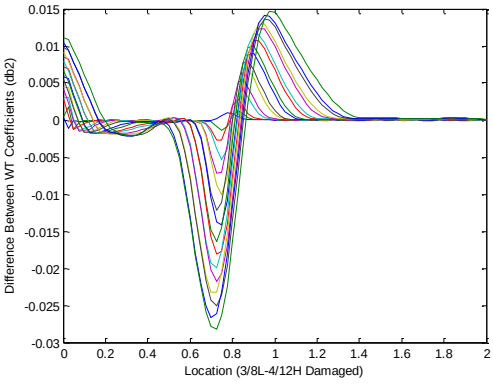

(d) 4/12H damaged

Fig. 6 Wavelet coefficient differences (3/8L, db2)

As shown in the maximum curves, wavelet coefficient difference increases approximately linearly with the scale increasing for each damage case. Instead, the maximum

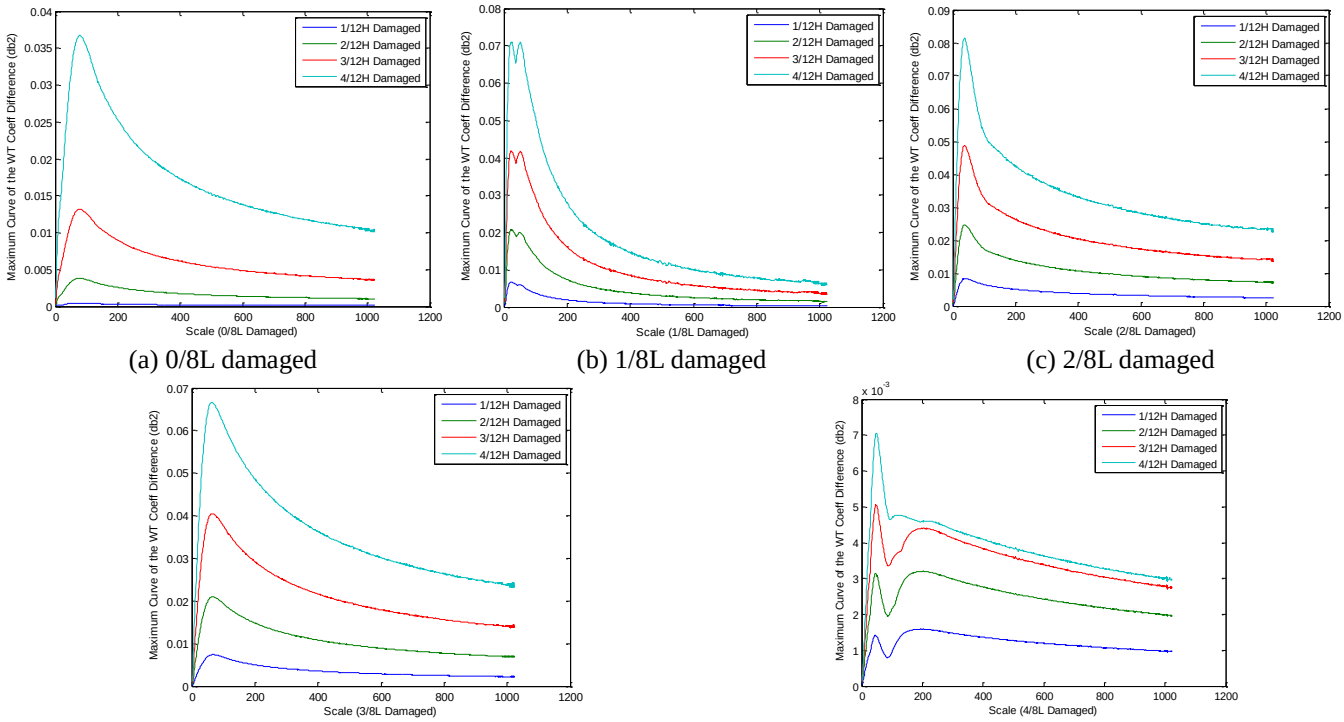

(a) 0/8L damaged (b) 1/8L damaged (c) 2/8L damaged

(d) 3/8L damaged (e) 4/8L damaged

Fig. 7 Maximum curve of wavelet coefficient differences (db2)

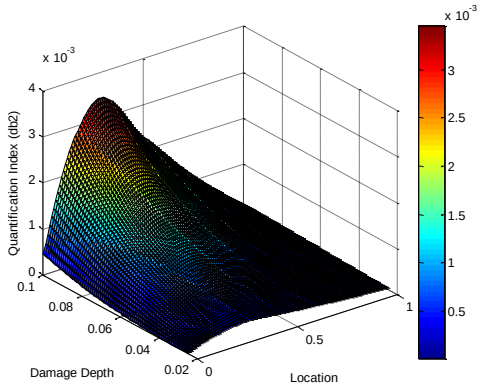

Fig. 8 Damage quantification index (db2)

curve of the mode shape wavelet transform coefficient differences can directly describe the *Lipschitz* related index, i.e., the secant slope through the point of origin and the maximum point of the maximum curve of the mode shape wavelet transform coefficient differences. Thus, the damage index based on structural mode shapes ($DI_{mode\ shape}$) can be defined as follow

$$DI_{mode\ shape} = \frac{\Delta W_f}{a}\Big|_{\Delta W_f = max\{\Delta W_f\}} \tag{20}$$

Where: a herein is the extreme scale and the corresponding ΔW_f at scale a is the maximum. Before ΔW_f reaches the maximum of the curve of wavelet transform coefficient differences, the curve is approximately linear. By this definition, the secant slope can be expressed as the quotient of ΔW and a, when ΔW_f reaches a maximum peak value.

By connecting the maximum of wavelet coefficient difference of the mode shape at each specific scale forming a maximum curve, we can quantify the damage extents with the proposed damage index, i.e., the secant slope through the origin and the maximum value of the maximum curve.

The accuracy of damage identification is the probability of the damage range to be identified, within which the maximum of the maximum curve is located, and the precision error for the accuracy of damage identification can be defined as follows

$$Err = \frac{L_{cal} - L_{targ}}{L_{beam}} \times 100\% \tag{21}$$

Where: Err is the identification precision estimation error, L_{cal} is the calculated interval for damage identification, and L_{targ} is the targeted interval for damage identification, and L_{beam} is the length of the beam.

Assuming that for a specific damage case, the maximum of wavelet transform coefficient differences is mostly distributed within the coordinate interval of damage to be identified, thus, we define the adjacent ranges as the targeted damage location, and also make error estimation correspondingly. Table 4 shows mode shape based damage identification results. (Eqs. (20)-(21)).

Based on the values of damage quantification index (damage locations are discretely distributed along the beam) as shown in the tables above, 3D fitting curves are plotted to intuitively reflect the relative and absolute values of damage quantification index in Fig. 8, in which case the damage occurs continuously. The distribution of corresponding damage localization accuracy is shown in Fig. 9.

Table 4 Damage localization & quantification (db2)

Damage Location	Damage Depth	Extreme Scale	Maximum	Damage Quantification Index	Damage Localization Accuracy	Damage Identification Error
0/8L	1/12H	19	2.23e-04	1.17e-05	95.45%	1.25%
	2/12H	76	0.0038	5.03e-05	25.32%	2.50%
	3/12H	79	0.0132	1.67e-04	24.39%	1.25%
	4/12H	79	0.0367	4.65e-04	21.95%	1.25%
1/8L	1/12H	23	0.0067	**2.91e-04**	**88.46%**	2.50%
	2/12H	23	0.0207	**9.01e-04**	**88.46%**	2.50%
	3/12H	23	0.0419	**0.0018**	**88.46%**	2.50%
	4/12H	21	0.0707	**0.0034**	**91.67%**	2.50%
2/8L	1/12H	40	0.0084	**2.10e-04**	**93.02%**	2.50%
	2/12H	37	0.0247	**6.68e-04**	**92.50%**	3.75%
	3/12H	36	0.0489	**0.0014**	**92.31%**	3.75%
	4/12H	36	0.0815	**0.0023**	**92.31%**	3.75%
3/8L	1/12H	67	0.0074	**1.10e-04**	**95.71%**	2.50%
	2/12H	66	0.0210	**3.18e-04**	**95.65%**	3.75%
	3/12H	64	0.0405	**6.32e-04**	**95.52%**	3.75%
	4/12H	62	0.0666	**0.0011**	**95.38%**	3.75%
4/8L	1/12H	45	0.0014	3.15e-05	47.92%	7.50%
	2/12H	46	0.0031	6.85e-05	42.86%	7.50%
	3/12H	47	0.0051	1.08e-04	38.00%	7.50%
	4/12H	48	0.0070	1.47e-04	35.29%	7.50%

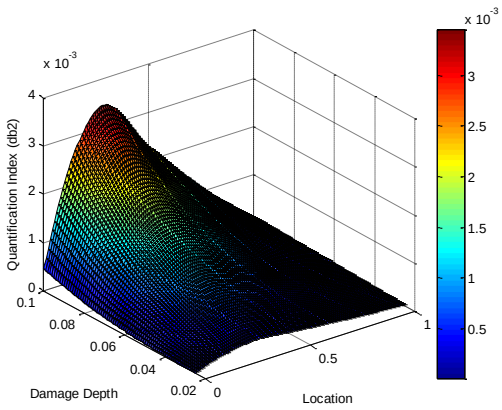

Fig. 9 Damage localization accuracy (db2)

Damage localization accuracy is more effective and damage quantification index is more sensitive within the central half of the entire damage range to be identified, and the values of WCD at a relatively small scale, are approximately equivalent to the secant slopes of WCD curves due to the linear relationship between WCD and the accordingly smaller scale, for different damage cases can be used as a roughly relative estimation for the damage quantification.

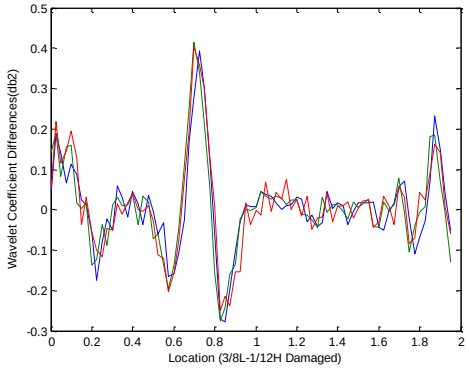

(a) 1/12H damaged

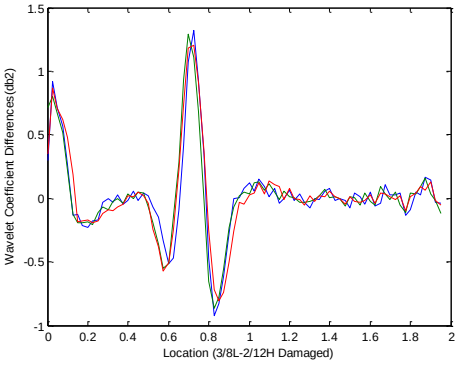

(b) 2/12H damaged

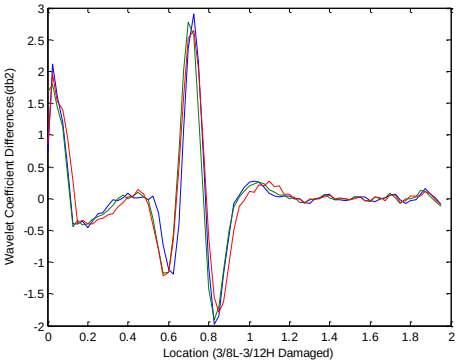

(c) 3/12H damaged

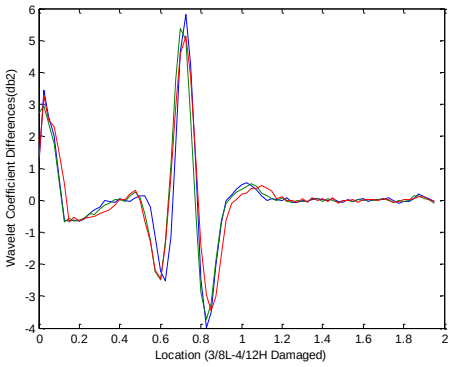

(d) 4/12H damaged

Fig. 10 Wavelet coefficient differences (3/8L, db2)

3. Modal curvature based damage identification

Since damage is regarded as localized stiffness reduction in a beam structure by utilizing modal curvature difference, the wavelet based method is found useful in detecting and localizing damages in beam models with different boundary conditions (Dawari and Vesmawala 2013). An aluminum beam with a single crack and a carbon fiber reinforced polymer composite beam with three cracks were experimentally verified for demonstrating the effectiveness of this approach (Cao *et al.* 2016).

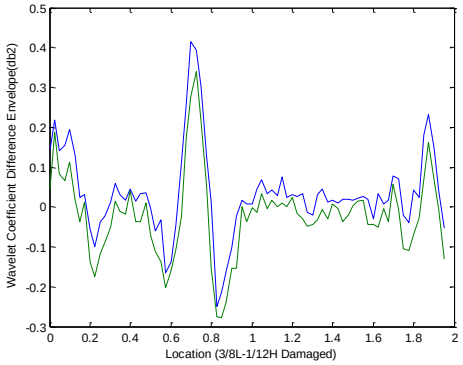

(a) 1/12H damaged

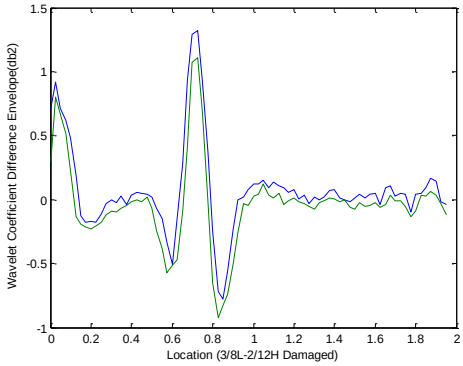

(b) 2/12H damaged

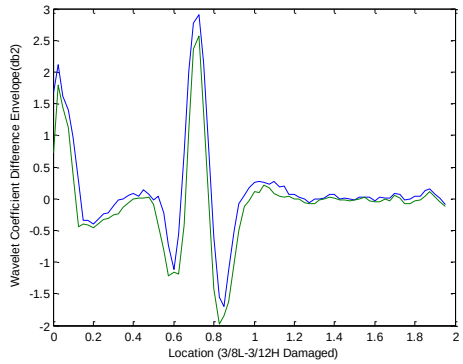

(c) 3/12H damaged

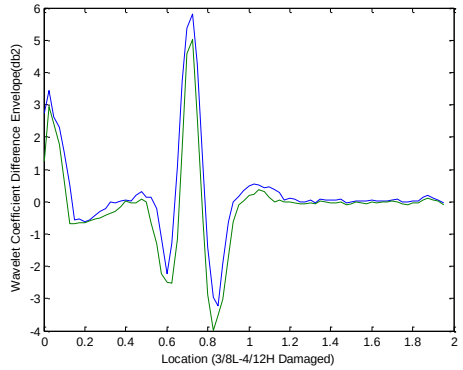

(d) 4/12H damaged

Fig. 11 Wavelet coefficient difference envelope (3/8L, db2)

To overcome the drawback that the curvature mode shape is susceptible to measurement noise, the synergy between a wavelet transform and a Teager energy operator was explored to improve the identification capability for multiple damage in noisy environment. Similar approach

Table 5 Damage localization & quantification (db2)

Damage Location	Damage Depth	Extreme Scale	Max.	Damage Quantification Index	Damage Localization Accuracy	Damage Identification Error
0/8L	1/12H	6	0.2312	**0.0385**	**96.09%**	2.50%
	2/12H	6	0.8486	**0.1414**	**99.22%**	2.50%
	3/12H	6	2.3752	**0.3959**	**92.97%**	2.50%
	4/12H	4	6.8836	**1.7209**	**100.00%**	3.25%
1/8L	1/12H	17	0.8452	**0.0497**	**98.63%**	5.00%
	2/12H	10	2.7611	**0.2761**	**98.83%**	3.25%
	3/12H	8	6.7453	**0.8432**	**99.41%**	3.25%
	4/12H	8	13.5891	**1.6986**	**99.61%**	3.25%
2/8L	1/12H	10	0.7192	**0.0719**	**95.51%**	3.25%
	2/12H	10	2.3336	**0.2334**	**98.83%**	3.25%
	3/12H	9	5.3641	**0.5960**	**99.61%**	3.25%
	4/12H	8	11.0142	**1.3768**	**99.61%**	3.25%
3/8L	1/12H	10	0.4038	**0.0404**	**93.75%**	3.25%
	2/12H	10	1.2026	**0.1203**	**98.83%**	3.25%
	3/12H	9	2.7741	**0.3082**	**99.41%**	3.25%
	4/12H	8	5.8027	**0.7253**	**99.41%**	3.25%
4/8L	1/12H	8	0.0970	**0.0121**	**85.35%**	6.25%
	2/12H	9	0.1428	**0.0159**	**87.30%**	6.25%
	3/12H	11	0.1874	**0.0170**	**87.70%**	6.25%
	4/12H	8	0.3378	**0.0422**	**87.11%**	6.25%

was applied to 2D curvature mode shapes for plates under noisy condition as well (Cao *et al.* 2014). Wavelet analysis was also performed in a damaged beam model for displacement, rotation and curvature mode shapes, and was tested and verified both in static or dynamic displacement profiles (Xu and Cao 2015, Prasad *et al.* 2006).

3.1 Central difference method

Since the modal curvature is relatively more sensitive to mode shape of a beam structure, we employ modal curvature of the beam as an analytic quantity, which is defined by using the second order derivative of the mode shape of the beam as follow

$$-\frac{M}{EI(x)} = W''(x) \approx \frac{W(x-h) - 2W(x) + W(x+h)}{h^2} \tag{22}$$

Where: M is the bending moment, EI is the bending stiffness with E the Young's modulus and I the moment of inertia, and W and W'' are respectively the mode shape and the modal curvature of the beam. W'' is approximately obtained by the second order central difference of W with the same interval h. The occurrence of damage will change the EI of the beam, which also causes discontinuity in W'', and subsequently, the discontinuity indicated in W'' manifests the presence of damage to some degree.

Similar to utilizing mode shapes in wavelet analysis, we also demonstrate how to use wavelet coefficient differences with respect to the modal curvature of the beam in Fig. 10. Herein, we choose wavelet scale 8-12 as an example, and to

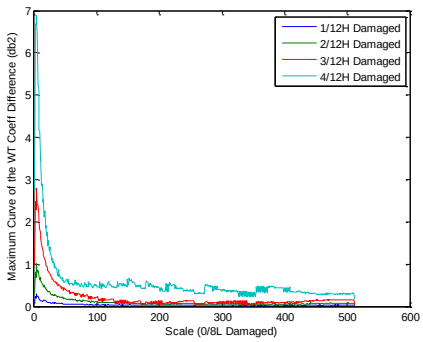

(a) 0/8L damaged

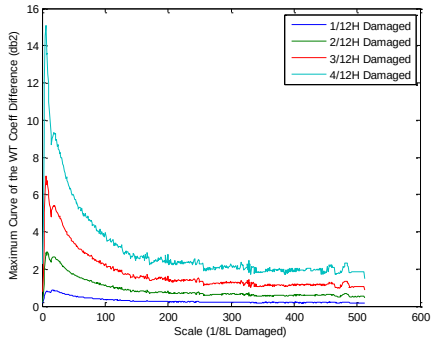

(b) 1/8L damaged

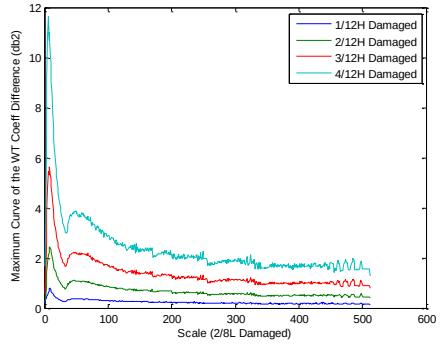

(c) 2/8L damaged

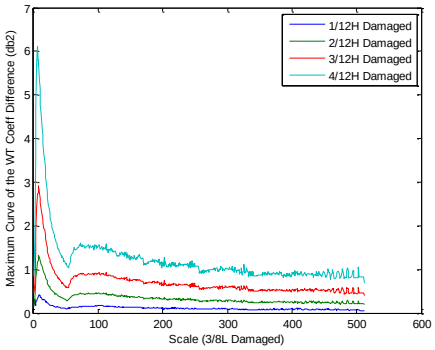

(d) 3/8L damaged

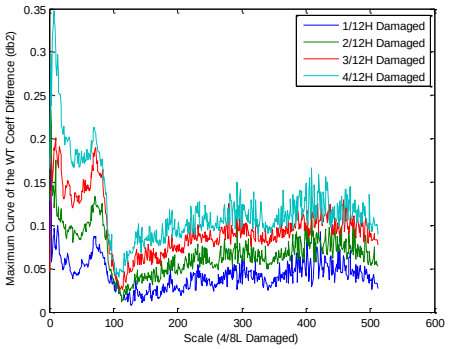

(e) 4/8L damaged

Fig. 12 Maximum curve of wavelet coefficient differences (3/8L, db2)

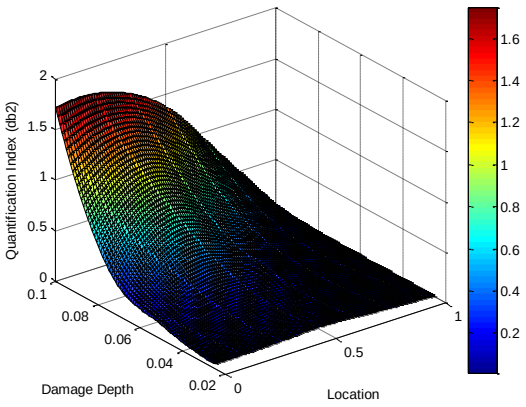

Fig. 13 Damage quantification index (db2)

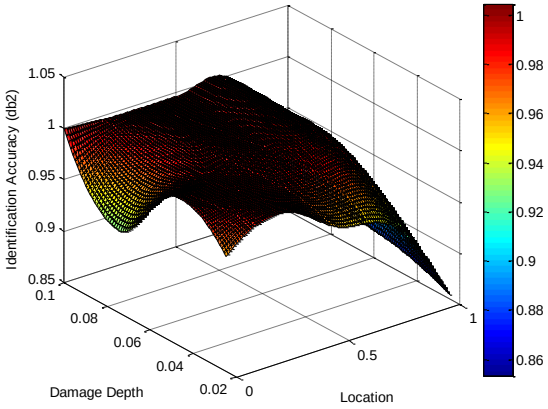

Fig. 14 Damage localization accuracy (db2)

make it clearer we use the envelope of the wavelet coefficient difference regarding modal curvatures in Fig. 11.

By calculating the wavelet coefficient differences of modal curvature maximum curves for both undamaged and damaged structure, we acquire the maximum curve variation tendency from wavelet scale 1:512 in Fig. 12.

Similar to mode shapes, according to different damage conditions, we calculate the extreme scale and the corresponding maximum, damage quantification index (*DI* modal curvature), damage localization accuracy and damage identification error. Table 5 shows curvature mode based damage identification results. (Eqs. (21), (23))

$$DI_{modal\ curvature} = \frac{\Delta W_f}{a}\Big|_{\Delta W_f = max\{\Delta W_f\}} \tag{23}$$

Based on the values of damage quantification index (damage locations are discretely distributed along the beam) as shown in the tables above, 3D fitting curves are plotted to intuitively reflect the relative and absolute values of damage quantification index in Fig. 13, in which case the damage occurs continuously. The distribution of corresponding damage localization accuracy is shown in Fig. 14.

3.2 Wavelet based damage identification

The weakness of wavelet based damage identification is that, the maximum peak of wavelet coefficient curve might drift as the analytical scale increases, thus, giving rise to relative inaccuracy of damage localization. Based on the characteristics of wavelet transform convolution operation, as discussed above, we can identify the detailed location of the occurred damage within the beam by choosing the

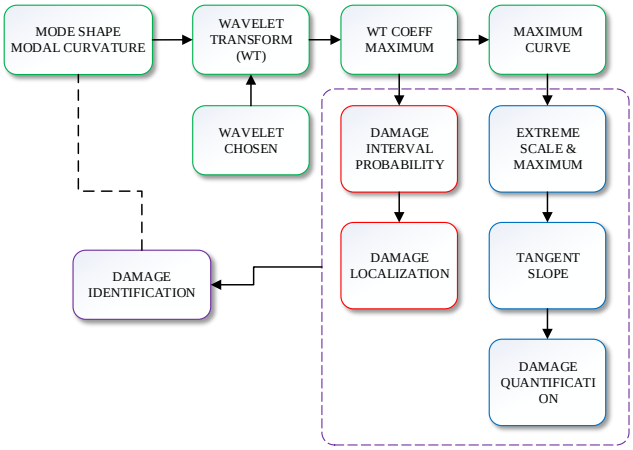

Fig. 15 Damage identification algorithm

maximum peak / one of the maximum peaks of the curve (if exists), where the wavelet coefficient difference curve reaches a maximum. Only when localization of damage is within the error limit can we follow up to quantify the damage extents based on the maximum curve of the differences of wavelet coefficients. The algorithm of mode shape based damage identification developed in this work is shown in Fig. 15.

4. Fuzzy pattern recognition and health state evaluation

More recently, several research studies have demonstrated promising results for development of an effective damage detection by integrating wavelet transform and artificial intelligence based methods such as artificial neural network. Some of the promising work in this regard are summarized below.

An optimal ANN architecture was recently established to detect damage occurrence with good accuracy. This algorithm can provide damage quantification with reasonable accuracy for the ASCE benchmark structure. In this approach, the ANN is for computing the wavelet energy of acceleration signals acquired from the structure, where the wavelet energy is used as damage feature to classify damage states of the structure (Reda 2010).

An algorithm encompassing artificial neural networks coupled with wavelet multi-resolution analysis were also utilized for damage detection purposes by processing the structural dynamic response monitored by a group of accelerometers (Lucero and Taha 2005). Another method was introduced to improve pattern recognition and ambiguous damage detection for a pre-stressed concrete bridge by supplementing intelligent structural health monitoring with fuzzy sets Bayesian updating (Taha and Lucero 2005). With wavelet transform algorithm filtering random noise, ANFIS was found to model the structural behavior properly and to be an effective model updating technique to quantify damage index accurately when acquiring the structural response signal and the excitation data (Zhu *et al.* 2013). A structural damage identification method was further proposed by combining 2D wavelet transform for changing the structural vibration response signal in the 2D space, and the adaptive network-based fuzzy inference system (ANFIS) used to describe specific damage classification (Escamilla-Ambrosio *et al.* 2011).

A damage detection method based on wavelet packet was presented by exerting a vertical impact load on the surface of an arch bridge. The acceleration response of both the undamaged and damaged arch bridges were converted to node energy by using wavelet packet transform, achieving the effectiveness of damage identification (Guo *et al.* 2012). The dynamic testing of an old steel bridge was carried out using accelerometers for the damaged state and after partial retrofitting. The comparison was carried out using power spectral density, short-time Fourier transform, and wavelet packet transform related to the upstream and downstream trusses in the bridge (Walia *et al.* 2015). A dynamic fuzzy wavelet neural network approach was employed as a nonparametric system identification model to predict the structural response for damage evaluation. A Bayes factor evaluation metric was proposed to provide quantitative measure for assessing the accuracy of system identification and the state of global health of structures. (Jiang *et al.* 2007, Jiang *et al.* 2008)

4.1 Model introduction

In the work presented in this paper a hybrid approach for damage pattern recognition based on a fuzzy pattern recognition, and an artificial neural network, combined with wavelet multi-resolution analysis is introduced. As demonstrated in the following section, this approach shows superior results compared with those presented earlier for the damage detection study of a reinforced concreter beam.

An external transient load F=200 N is imposed at 3/4L along the beam, and we sample the points interspersed along the beam during a specific time period. This time period is used to acquire as much information as possible of the healthy structure, from which we will infer damage state, and future events or knowledge will be used to update the assessments yielding a reliable recognition of damage. Progressively low and high frequency components are decomposed from the dynamic signal using wavelet multi-resolution analysis (WMRA). These observations represent extracted features of the dynamic signals and are used to calculate an energy index. The energy index determines the level of structural health and these different health states can be classified using fuzzy pattern recognition. By establishing such fuzzy damage states based on the quantity of statistics and data updating, the damage pattern recognition completed not only can be used for damage warning but can also be related to structural reliability and safety with high confidence.

During a time period of healthy structural performance, neural network is trained to map the relationship “features” of the relatively healthy structural dynamics. Signals acquired from the beam are decomposed using wavelet multi resolution analysis. ANN is used to learn both the approximation and detail parts of the decomposed signal from the interspersed locations along the structure. The training process is performed during the healthy performance and ANN model is built to predict healthy

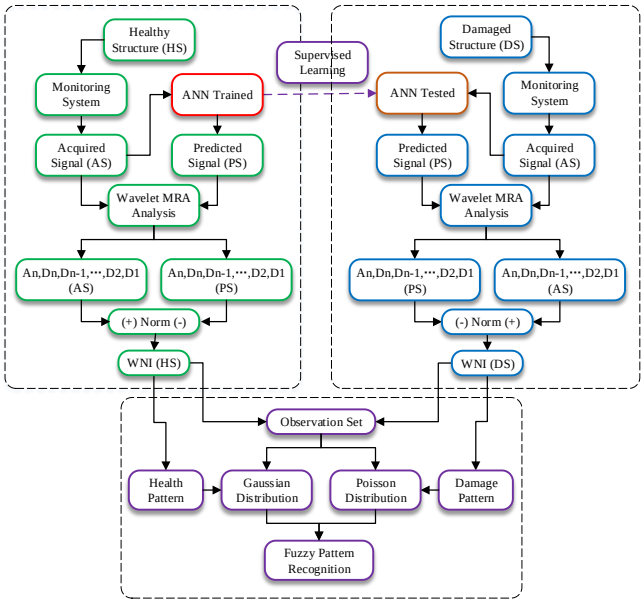

Fig. 16 WMRA based fuzzy pattern recognition module

structural response accordingly. For the unknown structural performance, the combined WMRA and ANN will yield mainly damage detection module. The schematic representation of the proposed damage detection module makes it possible to extract features from the signal and therefore, recognize the differences between the healthy and damaged patterns, and hence, the severity of the damage (see Fig. 16).

The error signal representing the error between the predicted and the acquired signal is computed in the wavelet domain by subtracting the wavelet coefficients of the predicted signal form the corresponding wavelet coefficients of the acquired signal at different resolution levels.

$$C_{ec} = C_{ac} - C_{pc} \tag{24}$$

$$C_{ec} = \left[\left|a_{(j)ec}\right|d_{(j)ec}\left|d_{(j-1)ec}\right|\cdots\cdots d_{1ec}\right] \tag{25}$$

$$WNI_N = \left[\sum_k \left|a_{(J)ec}(k)\right|^2 + \sum_k \sum_{j=1}^{J} \left|d_{(J)ec}(k)\right|^2\right] \tag{26}$$

Where: a is the approximation coefficient, d is the details coefficients, and j represents the level of wavelet decomposition. k is the number of samples observed during the specific time period. The energy index is the sum of all the decomposition coefficients of error signal. As Parseval's theorem relates the norm of the wavelet coefficients to the energy of the signal.

The difference between the damaged and healthy conditions can thus be established by evaluating *WNI* that represents the energy of the error signal at various operating instances. It can also be argued that the larger the difference the higher the level of damage in the structure. As the WA_NN module is trained to predict the system dynamics under healthy conditions, the *WNI* of the error signal shall be relatively constant during healthy operations. Also, the presence of new superimposed dynamic components will

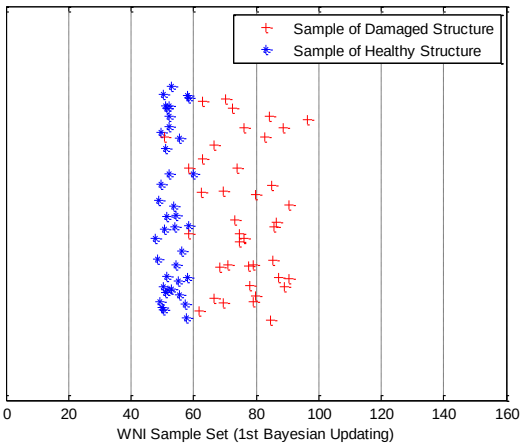

Fig. 17 WNI sample (1st Bayesian updating)

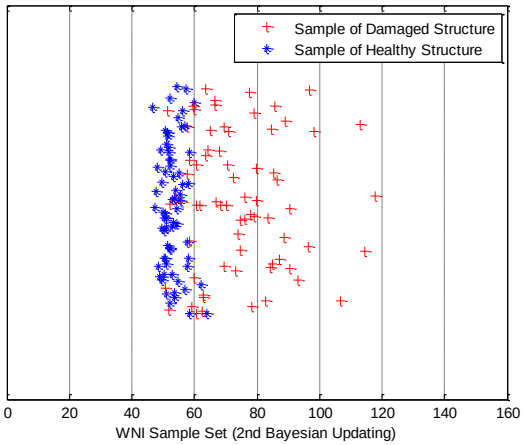

Fig. 18 WNI sample (2nd Bayesian updating)

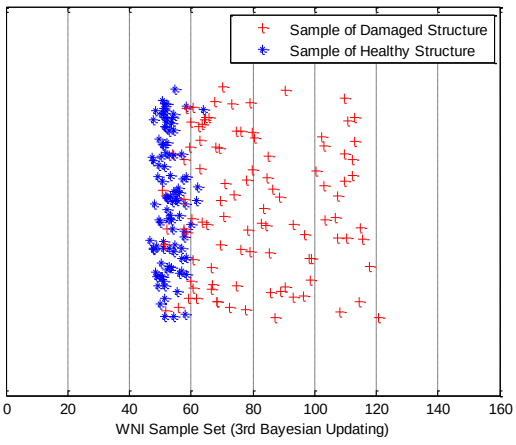

Fig. 19 WNI sample (3rd Bayesian updating)

account for an increase in the difference between the predicted and acquired signals indicated by the *WNI* of the error signal. This change in the *WNI* would suggest an occurrence of damage. It has been shown that changes in *WNI* can be linked to damage by observing the probability of *WNI* derived from subsequent healthy instances.

The followings are the sample collection of *WNI* for both healthy and damaged structure are presented in Tables 6 and 7. Note that the green background indicates the 1st

Table 6 WNI (Healthy structure)

52.42	51.00	52.05	52.98	51.60	50.15	55.64	52.22	53.96	49.46
52.32	48.40	52.72	49.56	50.38	59.74	48.87	57.28	50.89	54.34
50.36	58.48	53.63	51.48	55.63	50.73	58.45	51.85	58.19	49.81
47.83	57.66	55.17	50.88	54.31	56.16	51.25	58.11	52.26	49.25
52.32	51.57	46.49	57.52	50.18	51.17	47.37	53.18	54.81	56.16
50.94	63.97	54.76	51.68	54.20	52.16	52.31	53.74	55.98	61.95
53.65	48.23	50.61	57.09	57.00	49.63	50.55	52.82	53.32	50.69
47.77	51.59	56.81	54.99	51.61	49.59	49.93	48.87	56.29	52.31
51.73	58.56	54.45	61.87	53.42	47.80	56.79	53.97	48.62	50.88
51.96	54.28	58.57	52.56	54.49	47.59	51.44	49.12	54.11	52.99

Table 7 WNI (Damaged structure)

68.27	77.92	79.69	69.54	79.90	84.47	88.61	79.06	85.35	73.13
90.66	89.06	84.16	69.49	96.31	76.01	85.87	79.20	87.31	86.48
72.29	90.57	74.72	74.55	82.73	70.98	66.38	70.09	84.97	77.67
76.28	61.91	58.28	74.05	62.63	66.42	62.78	58.35	50.56	62.90
52.27	68.05	59.89	63.63	60.82	55.89	59.70	57.59	65.02	59.87
51.44	60.58	63.66	67.01	59.25	51.82	54.07	57.70	64.47	60.60
96.83	98.19	83.62	106.77	93.18	113.02	78.38	117.63	70.63	114.53
112.08	64.67	112.21	98.61	80.68	103.42	109.67	69.12	99.04	113.13
68.34	103.18	102.31	60.24	65.78	107.60	109.57	103.11	110.80	109.53
120.87	93.03	108.02	110.59	67.49	115.42	107.53	57.70	114.74	100.49

Bayesian updating, blue background the 2nd Bayesian updating, and pink background represents the 3rd Bayesian updating. (see Figs. 17-19).

4.2 Establishing fuzzy health patterns

Four structural health patterns (damage levels) ranging from healthy to significantly damage are proposed. The non-distinct boundaries between these health patterns and the inherent overlap make the system a suitable candidate for damage pattern recognition. We begin with the "Healthy" pattern, and the structural health membership function is defined as a left-shouldered fuzzy set using the Gaussian function described as follow

$$\mu_H(x) = \begin{cases} exp\left[\dfrac{-(x-\overline{WNI_H})}{\sigma^2_{WNI_H}}\right] & x \geq \overline{WNI_H} \\ 1 & x < \overline{WNI_H} \end{cases} \quad (27)$$

Our universe of discourse is all the WNI values. $\mu_H(x)$ represents the membership function of a fuzzy structural healthy pattern that has an average observed wavelet energy index $\overline{WNI_H}$ and a standard deviation of $\sigma^2_{WNI_H}$. Consequently, information from this first fuzzy set will be used to develop the proximate fuzzy set "Little Damage". We can locate the lower bound of "Little Damage" with the mean of "Healthy" $\overline{WNI_H}$, and we know the next fuzzy set will have higher WNI values than the mean for "Healthy". As such, Jeffrey's prior skews our initial assessment as a membership function to higher WNI mean values using equation

Jeffrey's non-informative prior density: $p(\lambda) = \frac{1}{\sqrt{\lambda}}$ (28)

Therefore, for the three damage levels beyond the "Healthy" set, this non-informative prior will be used as an initial estimate for that particular damage level. Subsequently, as information about the structural response becomes available, these Jeffrey's priors will update the membership function by mimicking the shape of the Poisson density function as the following equation

Poisson density function: $f(y|\lambda) = \frac{\lambda^y}{y!} exp(-\lambda)$ (29)

Where: λ represents the mean *WNI* value.

This algorithm goes a step further in the accommodation of uncertainty by using interval data to update the damage level membership functions. Therefore, the interval likelihood function which can be thought of as the strength of the fuzzy set (Eq. (30)) is used to update the membership function in a Bayesian sense as the posterior density of Eq. (31)

Interval Likelihood Function (strength of fuzzy set):

$$f([y_1, y_2]|\lambda) = \sum_{y=y_1}^{y_2} \frac{\lambda^y}{y!} exp(-\lambda) \quad (30)$$

Posterior Density Function (single observation):

$$f_1([y_1, y_2]|\lambda) = \frac{exp(-\lambda)\sum_{y=y_1}^{y_2} \frac{\lambda^{y-1/2}}{y!}}{\sum_{y=y_1}^{y_2} \frac{\Gamma(y+1/2)}{y!}} \quad (31)$$

Posterior Density Function (multiple observation):

$$f_i([y_1, y_2]|\lambda) = \frac{exp(-\lambda)\sum_{y=y_1}^{y_2} \frac{\lambda^y}{y!} * f_{i-1}}{\sum_{y=y_1}^{y_2} \frac{\Gamma(y)}{y!}} \quad (32)$$

Where: $[y_1, y_2]$ is i^{th} observation interval.

To summarize, *WNI* values over a time period will be used to develop the fuzzy set, "Healthy." In succession, the lower bounds for the remaining fuzzy sets will use the shape of Jeffrey's non-informative prior in posterior updating of a Poisson distribution. Using interval data within the bounds set forth by experts, the fuzzy damage sets, "Little," "Moderate," and "Significant" will be developed using Eqs. (30), (31) and (32) (see Figs. 20-23).

Table 8 Bayesian updating using interval data

Observation Sample	WNI (Healthy Structure)	WNI (Damaged Structure)			λ Value
		Little	Moderate	Significant	Critical
Initial Estimation	$\mu = 25.50$ $\sigma^2 = 5.00$	40.00		-	-
1st Bayesian Updating	$\mu = 52.94$ $\sigma^2 = 10.17$	66.70	83.92	-	-
2nd Bayesian Updating	$\mu = 53.05$ $\sigma^2 = 11.95$	61.79	81.78	106.18	-
3rd Bayesian Updating Fuzzy Set Established	$\mu = 52.98$ $\sigma^2 = 11.99$	62.07	79.58	96.66	111.87

Remark: Mean=0 in theory since ANN generalization ability is not good/noise influence, etc.

Table 9 *K*-means cluster analysis

Damage Level	Sample No.	Mean Value	Minimum	Maximum
Little	19	66.70	50.56	74.72
Moderate	21	83.92	76.01	96.31

Table 10 Class 1-little damage

68.27	69.54	73.13	69.49	72.29	74.72	74.55	70.98	66.38	70.09
61.91	58.28	74.05	62.63	66.42	62.78	58.35	50.56	62.90	

Table 11 Class 2-moderate damage

77.92	79.69	79.90	84.47	88.61	79.06	85.35	90.66	89.06	84.16
96.31	76.01	85.87	79.20	87.31	86.48	90.57	82.73	84.97	77.67
76.28									

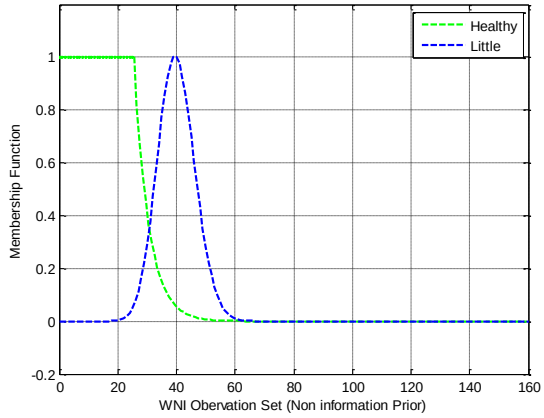

Fig. 20 Fuzzy sets (Non info prior)

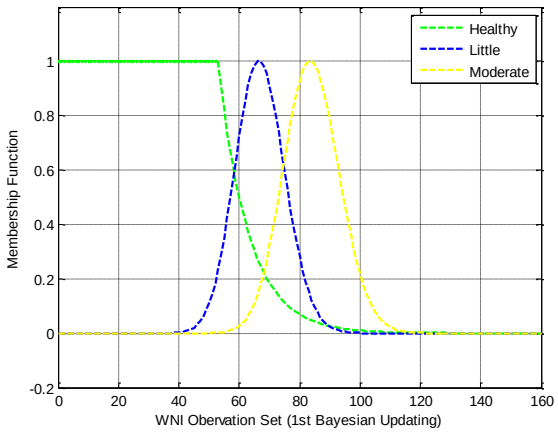

Fig. 21 Fuzzy sets (1st Bayesian updating)

Damage recognition is proposed by using fuzzy sets which determine different damage levels with wavelet norm index (*WNI*). A vector of WNI that represents consecutive measurements of vibration responses will be compared to defined damage levels (see Table 8).

Tables 9-11, Tables 12-15 and Tables 16-20 present the WNI (Damaged Structure) of 1st, 2nd and 3rd Bayesian Updating respectively.

In the Bayesian updating process, we assume prior probability distribution of parameter is constant, thus posterior probability distribution is proportional to

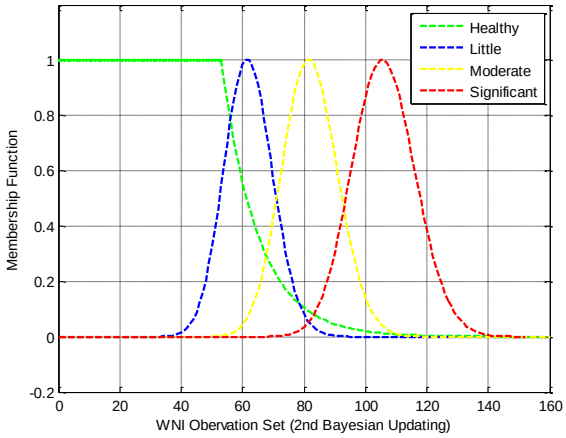

Fig. 22 Fuzzy sets (2nd Bayesian updating)

Table 12 *K*-means cluster analysis

Damage Level	Sample No.	Mean Value	Minimum	Maximum
Little	35	61.79	50.56	70.98
Moderate	28	81.78	72.29	93.18
Significant	7	106.18	96.31	117.63

Table 13 Class 1-little damage

68.27	69.54	69.49	70.98	66.38	70.09	61.91	58.28	62.63	66.42
62.78	58.35	50.56	62.90	52.27	68.05	59.89	63.63	60.82	55.89
59.70	57.59	65.02	59.87	51.44	60.58	63.66	67.01	59.25	51.82
54.07	57.70	64.47	60.60	70.63					

Table 14 Class 2-moderate damage

77.92	79.69	79.9	84.47	88.61	79.06	85.35	73.13	90.66	89.06
84.16	76.01	85.87	79.20	87.31	86.48	72.29	90.57	74.72	74.55
82.73	84.97	77.67	76.28	74.05	83.62	93.18	78.38		

Table 15 Class 3-significant damage

96.31	96.83	98.19	106.77	113.02	117.63	114.53

Table 16 *K*-means cluster analysis

Damage Level	Sample No.	Mean Value	Minimum	Maximum
Little	41	62.07	50.56	70.63
Moderate	25	79.58	70.98	87.31
Significant	16	96.66	88.61	103.42
Critical	18	111.87	106.77	120.87

Table 17 Class 1-little damage

68.27	69.54	69.49	66.38	70.09	61.91	58.28	62.63	66.42	62.78
58.35	50.56	62.90	52.27	68.05	59.89	63.63	60.82	55.89	59.70
57.59	65.02	59.87	51.44	60.58	63.66	67.01	59.25	51.82	54.07
57.70	64.47	60.60	70.63	64.67	69.12	68.34	60.24	65.78	67.49
57.70									

Table 18 Class 2-moderate damage

77.92	79.69	79.90	84.47	79.06	85.35	73.13	84.16	76.01	85.87
79.20	87.31	86.48	72.29	74.72	74.55	82.73	70.98	84.97	77.67
76.28	74.05	83.62	78.38	80.68					

Table 19 Class 3-significant damage

88.61	90.66	89.06	96.31	90.57	96.83	98.19	93.18	98.61	103.42
99.04	103.18	102.31	103.11	93.03	100.49				

Table 20 Class 4-critical damage

106.77	113.02	117.63	114.53	112.08	112.21	109.67	113.13	107.60	109.57
110.80	109.53	120.87	108.02	110.59	115.42	107.53	114.74		

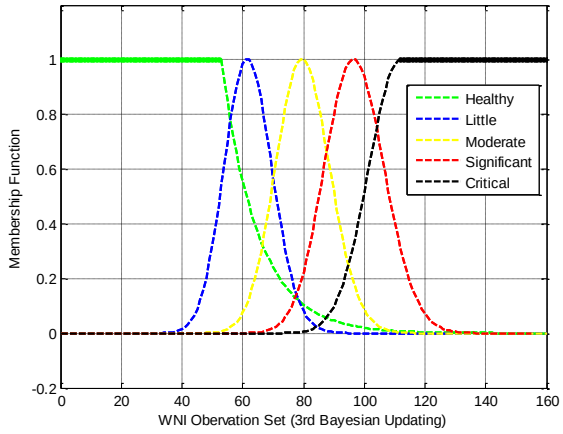

Fig. 23 Fuzzy sets (3rd Bayesian updating)

maximum likelihood function updated by data set, and meanwhile different fuzzy patterns (Healthy (H), Little (L), Moderate (M), Significant (S), Critical (C)) are established using WNI Observation Samples.

4.3 Damage recognition

Suppose in the discourse domain, 40, 42,…, 122 are what we select as the *WNI* observation set.

For each fuzzy pattern, choose ten discrete *WNI* values as representative observation values and calculate the degree of membership, which covers the main domain of each fuzzy set.

WNI_H = [40 42 44 46 48 50 52 54 56 58 …];
WNI_L = [… 50 52 54 56 58 60 62 64 66 68 …];
WNI_M = [… 68 70 72 74 76 78 80 82 84 86 …];
WNI_S = [… 86 88 90 92 94 96 98 100 102 104 …];
WNI_C = [… 104 106 108 110 112 114 116 118 120 122];

Calculate the value of membership function for each fuzzy set (FZY_H, FZY_L, FZY_M, FZY_S. FZY_C) accordingly.

FZY_H = [1.0000 1.0000 1.0000 1.0000 1.0000 1.0000 1.0000 0.9184 0.7773 0.6579 …];
FZY_L = [… 0.3207 0.4649 0.6244 0.7793 0.9061 0.9839 1.0000 0.9534 0.8543 0.7208 …];
FZY_M = [… 0.4199 0.5564 0.6966 0.8253 0.9267 0.9875 1.0000 0.9636 0.8845 0.7744 …];
FZY_S = [… 0.5551 0.6822 0.8013 0.9006 0.9693 1.0000 0.9898 0.9407 0.8592 0.7547 …];
FZY_C = [… 0.7462 0.8490 0.9303 0.9822 1.0000 1.0000 1.0000 1.0000 1.0000 1.0000];

We use *WNIT* as test sample, which will be input to the established fuzzy sets and we will get the membership of each sample *FZYT*.

Table 21 WNIT similarity metric (Correlation analysis)

WNI_H	WNI_L	WNI_M	WNI_S	WNI_C
0.2483	0.6574	0.6736	0.7794	0.7118

WNIT=[0 0 0…91.73 97.82 100.73 102.42 102.48 102.51 102.65 105.22 107.13 107.34 … 0 0 0];
FZYT=[0 0 0…0.6341 0.9422 1.0000 1.0000 1.0000 0.9903 0.9903 0.9435 0.8655 0.8655…0 0 0];

From Table 21, we can see that the test sample has a great approximation as "Significant Damage".

5. Conclusions

As presented in this paper, wavelet, artificial neural networks, and fuzzy theory have been applied as a novel approach employed in the intelligent Observe-Orientate-Decide-Act framework (Bedworth *et al.* 2000) for damage detection analysis of a reinforced concrete beam.

In recent years, a multi-disciplinary artificial intelligence based data fusion community has been emerging with promising applications in structural health monitoring. Therefore, the purpose of this paper was threefold. First a brief review of a series of work in wavelet analysis pertaining to structural health monitoring and damage detection was presented. Second, based on wavelet theory and its outstanding multi-resolution analysis property, we established a damage identification method utilizing mode shapes and modal curvature of beam structures, and further integrating that with a fuzzy pattern recognition approach for the damage detection of structures under dynamic loads. Most importantly, multiscale analysis using wavelet coefficient differences and selecting an optimal scale as a measurement of damage indexes based on mode shape and curvature mode were conducted. The third objective of this work was to demonstrate and postulate that the related theory and methodologies used in this case study as a novel approach for the damage detection in a beam structure can be extended and applied to other challenging problems in the field of structural health monitoring such as corrosion detection, fatigue analysis, reliability evaluation, data and information fusion, and decision analysis and control strategies (see Fig. 24).

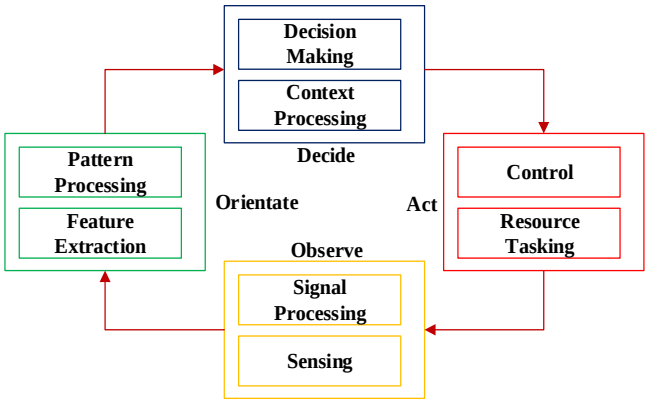

Fig. 24 Omnibus model for data fusion

References

Bedworth, M. and O'Brien, J. (2000), "The omnibus model: a new model of data fusion?", *IEEE Aerosp. Elec. Syst. Mag.*, **15**(4), 30-6.

Beheshti-Aval, S.B., Taherinasab, M. and Noori, M. (2013), "Some precautions to consider in using wavelet transformation for damage detection analysis of plates", *Smart Struct. Syst.*, **11**(1), 35-51.

Cao, M., Radzieński, M., Xu, W. and Ostachowicz, W. (2014), "Identification of Multiple Damage in Beams Based on Robust Curvature Mode Shapes", *J. Mech. Syst. Signal Pr.*, **46**(2), 468-480.

Cao, M.S., Xu, W., Ren, W.X., Ostachowicz, W., Sha, G.G. and Pan, L.X. (2016), "A concept of complex-wavelet modal curvature for detecting multiple cracks in beams under noisy conditions", *J. Mech. Syst. Signal Pr.*, **76**, 555-575.

Chang, P.C., Flatau, A. and Liu, S.C. (2003), "Health monitoring of civil infrastructure", *J. Struct. Hlth. Monit.*, **2**(3), 257-67.

Daubechies, I. (1990), "The wavelet transform, time-frequency localization and signal analysis", *IEEE Tran. Inform. Theory*, **36**(5), 961-1005.

Daubechies, I. (1992), *Ten Lectures on Wavelets. Philadelphia: Society for Industrial and Applied Mathematics*, Rutgers University.

Dawari, V.B. and Vesmawala, G.R. (2013), "Structural damage identification using modal curvature differences", *J. Mech. Civil Eng.*, **4**, 33-38.

Douka, E., Loutridis, S. and Trochidis, A. (2003), "Crack identification in beams using wavelet analysis", *J. Solid. Struct.*, **40**(13), 3557-3569.

Escamilla-Ambrosio, P.J., Liu, X., Lieven, N.A. and Ramirez-Cortes JM. (2011), "ANFIS-2D wavelet transform approach to structural damage identification", *Fuzzy Information Processing Society (NAFIPS), IEEE, 2011 Annual Meeting of the North American*, March..

Farouk, M.H. (2014), "Wavelets, wavelet filters, and wavelet transforms", *Appl. Wavel. Speech Pr.*, https://doi.org/10.1007/978-3-319-02732-6_3.

Guo, H., Lin, J. and Li, Z. (2012), "Structural damage localization of steel arch bridge based on wavelet packet transform", *Software Engineering and Knowledge Engineering: Theory and Practice 2012*, Springer Berlin Heidelberg.

Hera, A. and Hou, Z. (2004), "Application of wavelet approach for ASCE structural health monitoring benchmark studies", *J. Eng. Mech.*, **130**(1), 96-104.

Hong, J.C., Kim, Y.Y., Lee, H.C. and Lee, Y.W. (2002), "Damage detection using the Lipschitz exponent estimated by the wavelet transform: applications to vibration modes of a beam", *J. Solid. Struct.*, **39**(7), 1803-1816.

Hou, Z., Noori, M. and Amand, R.S. (2000), "Wavelet-based approach for structural damage detection", *J. Eng. Mech.*, **126**(7), 677-683.

Huang, Y., Meyer, D. and Nemat-Nasser S. (2009), "Damage detection with spatially distributed 2D continuous wavelet transform", *J. Mech. Mater.*, **41**(10), 1096-1107.

Jiang, X. and Mahadevan, S. (2008), "Bayesian probabilistic inference for nonparametric damage detection of structures", *J. Eng. Mech.*, **134**(10), 820-831.

Jiang, X. and Mahadevan, S. (2008), "Bayesian wavelet methodology for structural damage detection", *J. Struct. Control Hlth. Monit.*, **15**(7), 974-991.

Jiang, X., Mahadevan, S. and Adeli, H. (2007), "Bayesian wavelet packet denoising for structural system identification", *J. Struct. Control Hlth. Monit.*, **14**(2), 333-356.

Lee, D.T. (1994), "Yamamoto a. wavelet analysis: theory and applications", *Hewlett Pack. J.*, **1**, 45-44.

Loutridis, S., Douka, E. and Trochidis, A. (2004), "Crack identification in double-cracked beams using wavelet analysis", *J. Sound Vib.*, **277**(4), 1025-1039.

Loutridis, S., Douka, E., Hadjileontiadis, L.J. and Trochidis, A.A. (2005), "Two-dimensional wavelet transform for detection of cracks in plates", *J. Eng. Struct.*, **27**(9), 1327-38.

Lucero, J. and Taha, M.R. (2005), "A wavelet aided fuzzy damage detection algorithm for structural health monitoring", *Proceedings of the 23rd International. Modal Analysis Conference (IMAC)*, Orlando, Florida.

Mallat, S. and Hwang, W.L. (1992), "Singularity detection and processing with wavelets", *IEEE Tran. Inform. Theory*, **38**(2), 617-643.

Mallat, S.A. (1999), *Wavelet Tour of Signal Processing. Academic Press*, 2nd Edition, Elsevier Inc.

Masoumi, M.A. and Ashory, M.R. (2014), "Damage identification from uniform load surface using continuous and stationary wavelet transforms", *Latin Am. J. Solid. Struct.*, **11**(5), 738-754.

Nikravesh, S.M. and Chegini, S.N. (2013), "Crack identification in double-cracked plates using wavelet analysis", *Meccanica*, **48**(9), 2075-2098.

Prasad, B.R., Lakshmanan, N., Muthumani, K. and Gopalakrishnan, N. (2006), "Enhancement of damage indicators in wavelet and curvature analysis", *J. Sadhana*, **31**(4), 463-486.

Quek, S.T., Wang, Q., Zhang, L. and Ang, K.K. (2001), "Sensitivity analysis of crack detection in beams by wavelet technique", *J. Mech. Sci.*, **43**(12), 2899-2910.

Reda Taha, M.M. (2010), "A neural-wavelet technique for damage identification in the ASCE benchmark structure using phase II experimental data", *J. Adv. Civil Eng.*, **2010**, ID 675927, 13.

Rucka, M. and Wilde, K. (2006), "Crack identification using wavelets on experimental static deflection profiles", *J. Eng. Struct.*, **28**(2), 279-288.

Rucka, M.A. and Wilde, K.R. (2006), "Application of continuous wavelet transform in vibration based damage detection method for beams and plates", *J. Sound Vib.*, **297**(3), 536-50.

Taha, M.R. and Lucero, J. (2005), "Damage identification for structural health monitoring using fuzzy pattern recognition", *J. Eng. Struct.*, **27**(12), 1774-1783.

Walia, S.K., Patel, R.K., Vinayak, H.K. and Parti, R. (2015), "Time-frequency and wavelet-based study of an old steel truss bridge before and after retrofitting", *J. Civil Struct. Hlth. Monit.*, **5**(4), 397-414.

Wang, Q. and Deng, X. (1999), "Damage detection with spatial wavelets", , *J. Solid. Struct.*, **36**(23), 3443-3468.

Xu, W., Cao, M., Ostachowicz, W., Radzieński, M. and Xia, N. (2015), "Two-dimensional curvature mode shape method based on wavelets and teager energy for damage detection in plates", *J. Sound Vib.*, **347**, 266-78.

Xu, Y.F., Zhu, W.D., Liu, J. and Shao, Y.M. (2014), "Identification of embedded horizontal cracks in beams using measured mode shapes", *J. Sound Vib.*, **333**(23), 6273-6294.

Zhao, Y. and Noori, M. (2017), "Mode shape-based damage identification for a reinforced concrete beam using wavelet coefficient differences and multiresolution analysis", *J. Struct. Control Hlth. Monit.*, DOI: 10.1002/stc.2041

Zhu, F., Deng, Z. and Zhang, J. (2013), "An integrated approach for structural damage identification using wavelet neuro-fuzzy model", *J. Expert Syst. Appl.*, **40**(18), 7415-7427.

CC